JOURNAL OF MATERIALS SCIENCE 28 (1993) 2471–2480

Fracture tests in Mode I on fibre-reinforced plastics

E. K. TSCHEGG
Institut für Angewandte und Technische Physik, TU Wien, A-1040 Vienna, Austria
K. HUMER, H. W. WEBER
Atominstitut der Österreichischen Universitäten, A-1020 Vienna, Austria

The characterization of crack growth (Mode I) in glass fibre-reinforced materials is difficult because neither the crack length nor the crack tip can be assessed with sufficient accuracy because of delamination and bridging of broken and unbroken fibres. Hence linear elastic fracture mechanics cannot be employed. A new testing technique is reported, to characterize the crack growth in Mode I under quasistatic loading conditions in terms of fracture mechanics. The tests and evaluation procedures are based on the fracture energy concept, which does not require knowledge of the exact crack length. Experiments were performed at room temperature and 77 K, on a two-dimensionally glass fibre-reinforced epoxy (ISOVAL 10). The splitting test method proposed in the present work is experimentally simple; the loading device and the sample geometry are small and well suited for measurements at low temperatures on both unirradiated or irradiated samples. Results of acoustic emission and fractographic examinations, as well as investigations on the specimen-size dependence of the measured fracture mechanical quantities, are presented. Advantages and disadvantages of the new technique are discussed.

1. Introduction

Glass fibre-reinforced plastics have become very attractive for a variety of applications because of their excellent mechanical, electrical, non-magnetic and thermal properties, as well as due to their low weight. Because of their high strength, high stiffness-to-weight ratio and low thermal expansion coefficient, fibre-reinforced plastics have been employed as structural materials in many machines and technical devices, and in some cases even under special environments, such as elevated or cryogenic temperatures as well as gamma and/or particle radiation. In mechanical engineering, motorcar manufacturing and other technical applications, high durability and low wear of the components are needed at room temperature and elevated temperatures. New applications in low-temperature technology, aeronautics and space require adequate material performance down to cryogenic temperatures. Because of their non-magnetic and electrical insulation behaviour, fibre-reinforced plastics have become important as insulating and support materials for the windings of superconducting magnets, e.g. for nuclear fusion reactors. However, when fibre-reinforced plastics are employed in space as well as in nuclear technologies, the material will be exposed to a radiation environment consisting of gamma and/or particle radiation, and hence, adequate mechanical properties are also required in the presence of such radiation environments.

In view of the increasing number of these applications, the assessment of the mechanical properties of fibre-reinforced plastics both at elevated and low temperatures and under various loading conditions (e.g. tension, compression, shear and, in particular, in the crack opening mode) has become of special interest and is indispensable for further material development. In addition, a fracture mechanical characterization of the material is necessary for design purposes in order to predict reliably the performance of the components over the plant lifetime.

In order to deduce fracture mechanical quantities of homogeneous isotropic materials (e.g. metals, plastics, ceramics, etc.) several standardized test procedures and fracture mechanical concepts (K-, J-, R- or G-concept) exist. Fracture mechanical calculations based on these concepts require a certain material behaviour (e.g. linear elastic or linear elastic–ideal-plastic behaviour) as well as the accurate knowledge of the crack length. Whereas the exact location of the crack tip can be determined with sufficient accuracy for homogeneous isotropic materials, this is a serious problem for inhomogeneous anisotropic fibre-reinforced plastics. As can be seen in Fig. 1, the damage zone at the crack tip can be formed by various microscopic damage mechanisms (yielding and cracking of the matrix, debonding at the fibre/matrix interface; bridging, pull-out and failure of fibres), which masks the exact location of the real crack tip. Furthermore, fibre

0022–2461

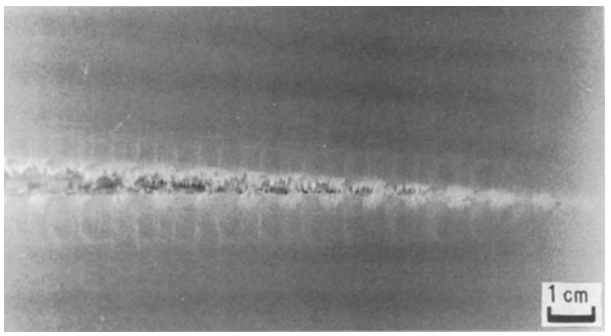

Figure 1 "Bridging" and pull-out of fibres around the crack tip in a fibre-reinforced material.

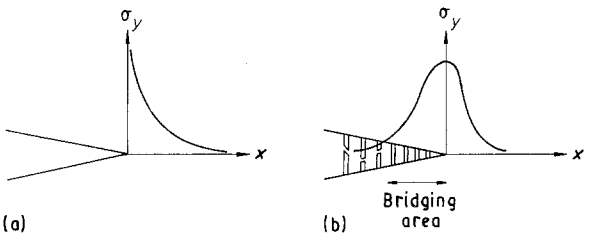

Figure 2 Schematic view of the stress distribution within (a) a "linear elastic" material and (b) a reinforced material.

bridging leads to a stress distribution around the crack tip which is different from a linear elastic or a linear elastic–ideal plastic material. Hence, the damage cannot be described with one of the above-mentioned fracture mechanical concepts. Fig. 2 shows a schematic view of these differences in material behaviour between a linear elastic and a fibre-reinforced material and emphasizes clearly that fracture mechanical concepts based on the linear elastic fracture mechanism (LEFM) are not suitable for fibre-reinforced plastics.

In the past, several models, test methods and specimen geometries have been proposed and considerable progress has been made in applying fracture mechanical concepts to describe the crack growth process in Mode I in fibre-reinforced plastics. A brief summary may be given as follows.

Lau *et al.* [1] measured the interlaminar fracture energy in Mode I of glass fibre-reinforced polyester at room temperature and 77 K by two different test techniques: the width-tapered double cantilever beam (WTDCB) and the wedge-splitting test (WST) method. On the basis of LEFM, both methods lead mathematically to the same fracture energy in approximate agreement with experiment. It should be pointed out that the measurement of the actual crack length is not necessary in the WTDCB test, but the experiment is complicated. On the other hand, the WST method is simple, but the crack length has to be determined. Lee [2] investigated the fracture toughness of various composites at room temperature in Mode I delamination (interlaminar failure) and transverse cracking (intralaminar failure) by the WTDCB and the double-torsion test. Although the fracture toughness values obtained from the two test methods were found to be quite comparable, the crack length is needed for both test methods to calculate the fracture toughness. The interlaminar fracture behaviour in Mode I was investigated on various types of carbon fibre-reinforced polyether and epoxy resin composites by Hashemi *et al.* [3, 4]. The data obtained from tests with DCB specimens at room temperature were analysed by several LEFM approaches (area method, linear-beam theory and compliance method). Garg [5] studied intra- and interlaminar failure modes in fibre-reinforced epoxy laminates at room temperature. On the basis of a LEFM approach with the compliance method, he investigated the interlaminar fracture energy and fracture toughness in Mode I delamination with the DCB specimen and Mode I transverse cracking (intralaminar failure) with the compact tension (CT) and the three-point bending (TPB) specimen. In addition, Garg and Ishai [6, 7] used acoustic emission (AE) methods in order to detect the crack initiation point and to identify Mode I delamination and Mode I transverse cracking.

Similar investigations on the fracture behaviour in Mode I of fibre-reinforced ceramic and metal matrix composites have been made by several researchers. Kagawa *et al.* [8] studied Mode I crack initiation and crack propagation of tantalum fibre-reinforced ceramic matrix composites at room temperature with TPB specimens. During the measurements the load versus displacement curves were recorded and the work of fracture was determined from the area under the load versus displacement curve. In addition, the total AE ringdown count rate was recorded, in order to investigate the fracture process of the composites. Daimaru *et al.* [9] and Jeng *et al.* [10] used TPB specimens made of carbon fibre-reinforced metal matrix and SCS fibre-reinforced titanium alloy matrix composites. The area under the recorded load versus displacement curves is considered to be equal to the total energy absorbed during the whole fracture process. This energy, divided by the lengths of both fracture surfaces, is denoted as the work of fracture or the macroscopic fracture surface energy. In addition, a theoretical model has been proposed to predict the work of fracture.

Considerable progress has been achieved by Aronsson and Bäcklund [11, 12] who compared experimental results obtained from TPB, single-edge notched and CT carbon fibre-reinforced epoxy matrix specimens with calculations based on three different models for predicting the strength of the composites. The semi-empirical "inherent flaw model" (IFM) as well as the "point stress criterion" (PSC) require different values of the characteristic length for various sizes of the notch. Furthermore, they do not account for the redistribution of stresses due to damage growth. A more general method, called the "damage zone model" (DZM) or the fracture energy concept, has been developed by Hillerborg [13, 14]. It requires only basic material properties (unnotched tensile strength, apparent fracture energy, composite stiffness) for predicting the strength of the composites. The fracture energy concept [13, 14] does not require knowledge of the

exact crack length for fracture mechanical calculations, and hence, can be used for fibre-reinforced plastics.

The main goal of the present study was the determination of fracture mechanical properties of fibre-reinforced plastics in the crack opening mode (Mode I) on the basis of the fracture energy concept [13, 14]. A new testing technique in combination with a simple and small specimen geometry has been developed, which permits an experimentally simple measurement of the fracture behaviour of unirradiated or irradiated samples at all temperatures down to cryogenic temperatures. The main results of the tests are load versus displacement curves, which contain all the information needed to characterize the fracture behaviour of the materials for numerical calculations.

2. Fracture energy concept

Whenever fibre-reinforced plastics with a notch are exposed to a load, a damage zone (fracture process zone) will be formed at the notch. The term "damage" is used here as a collective expression for various types of microscopic damage mechanisms (yielding and cracking of the matrix, debonding of the fibre/matrix interface, bridging, pull-out and fracture of fibres). As pointed out in the introduction, these damage mechanisms lead to a stress distribution around the crack tip, which is different from a linear elastic material (Fig. 2a,b). In order to simplify the calculations in the fracture energy concept, the damage zone is represented by a "fictitious crack" with cohesive stresses acting on its surfaces. Increasing damage growth results in increased crack opening and a reduction of the cohesive stresses, which corresponds to an increasing separation of the material. Aronsson and Bäcklund [11, 12] employed a linear relationship between the cohesive stresses and the crack opening, for calculations with the finite element model (FEM) which led to satisfactory results. In order to obtain a better approximation for the real fracture behaviour, a "bilinear" relationship between the cohesive stresses and the crack opening as described for concrete by Roelfstra [15] is used in the present study (Fig. 3).

It is important to note that the area under the cohesive stress versus crack opening curve (as well as the load versus deformation curve divided by the fracture surface area of the samples) is equivalent to the specific fracture energy, G_F, and that σ_0 is the (unnotched) tensile strength of the composite. G_F represents the sum of all energy contributions dissipated by the various microscopic failure mechanisms during the whole fracture process. It should be emphasized, that for calculations with FEM the damage zone is represented by the (bi) linear cohesive stress versus crack opening relationship, whereas the composite outside the damage zone is assumed to behave as a linear elastic material.

From an experimental point of view, the area under the measured load versus crack opening curve is considered to be equal to the total energy (work of fracture) absorbed during the whole fracture process. Dividing this energy by the fracture surface leads to the specific fracture energy, G_F. Hence, the experimental load versus crack opening curve contains all the information needed for an application of the fracture energy concept.

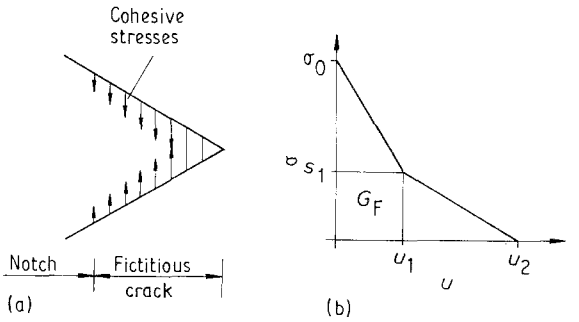

Figure 3 (a) Crack model with cohesive stresses and (b) assumed bilinear relation between the cohesive stress, σ, and the crack opening displacement (COD) u.

3. Materials, specimen geometry, testing procedure

In order to determine the fracture mechanical properties of fibre-reinforced plastics in the crack opening mode (Mode I) during stable crack growth conditions, a modified version of the wedge-splitting device, which has been employed successfully by Hillemeier [16] to measure the fracture toughness in Mode I on CT specimens made of concrete, in combination with a simple specimen geometry has been developed [17–19]. The principle of this test is the splitting of a specimen with a rectangular notch by means of wedges pressed between bearings on the top of the specimen. The wedge-loading device, as well as the specimen geometry are small and simple, and hence, very useful for measurements on both unirradiated and irradiated samples in the temperature range from elevated down to cryogenic temperatures [19].

The sample geometry is shown in Fig. 4a. It consists of a rectangular plate with a rectangular groove and a starter notch situated at the bottom of the groove. The specimens were cut from large plates of varying thickness (1, 1.5, 2 mm) of the laminate ISOVAL 10 (ISOVOLTA AG, Wiener Neudorf, Austria), which consists of a two-dimensional E-glass fabric (0°/90°) in epoxy (warp × woof: 17 × 8). The fibre orientation of the woven glass fabric was chosen to be parallel to both sides of the rectangular specimens. Before testing a sample the starter notch was always sharpened with a razor blade.

A schematic view of the test arrangement is presented in Fig. 4b and c. Two load transmission pieces (Fig. 4b) with bearings are placed into the groove. After inserting the wedge between the bearings, the force, F_M, can be transmitted from the testing machine to the specimen. The slender wedge (16.5°) produces a force on the bearings, which consists of two different components. The large horizontal force component, F_H, is the splitting force, which splits the specimen. If the wedge angle is small enough, the vertical force component, F_V, does not influence the test results.

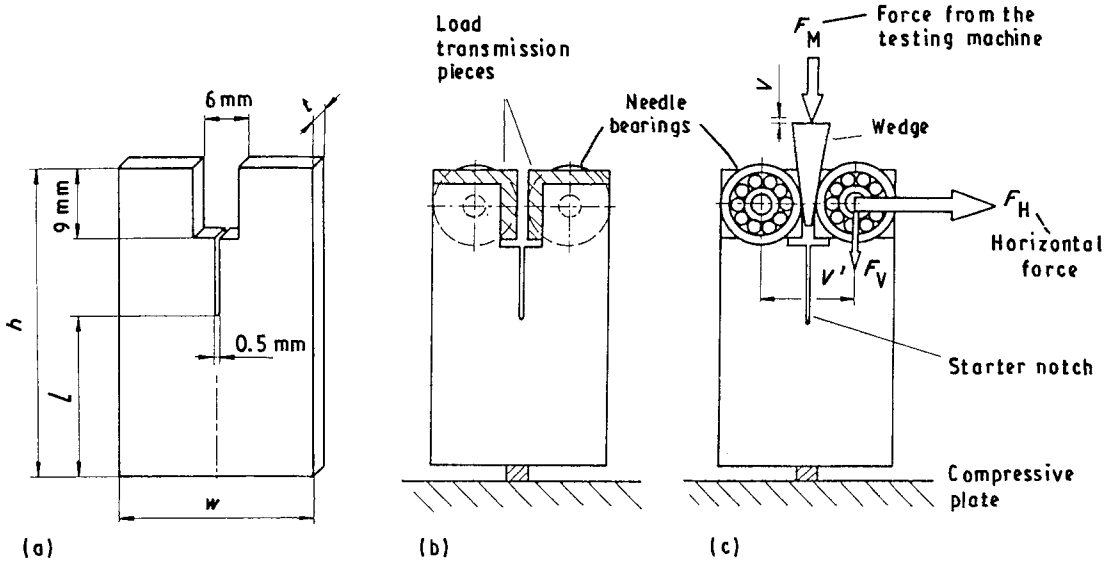

Figure 4 (a) Geometry and dimensions of the splitting test specimens and (b, c) schematic views of the test arrangement.

This has been verified by earlier investigations on concrete [20]. The load, F_M (Fig. 4c), is applied vertically on the bottom of the wedge using a stiff tensile testing machine provided with a force-reversal arrangement, in which the wedge-splitting device is placed on the support (i.e. a compressive plate, Fig. 4b, c). The choice of a small wedge angle leads to a reduction of the vertical load, F_M, relative to the horizontal splitting force, F_H, and hence, less elastic energy is stored in the specimen and in the loading device. Thus, an additional "artificial" increase of the stiffness of the testing machine compared to the specimen stiffness can be achieved. The wedge-splitting device and a specimen in the test position are shown in Fig. 5.

During measurements, both the vertical displacement, v, of the compressive plate and the applied load from the testing machine, F_M, were recorded on an XY recorder (load–deformation curve F_M versus v, F_M/v). The crosshead speed was set to be 0.5 mm min^{-1} throughout the experiments. The displacement v, which is perpendicular to the crack opening displacement (COD), v', is increased with respect to the COD, if a small wedge angle is chosen. v' can, therefore, be measured with sufficient accuracy. Details of the evaluation have been described elsewhere [21]. The horizontal force component, F_H, and the COD v' (Fig. 4c) are calculated from the following equations

$$F_H = F_v/2\tan\alpha \quad (1)$$

$$v' = 2v\tan\alpha \quad (2)$$

where α is the wedge angle and v is the vertical displacement of the compressive plate. As pointed out before, the area under the F_H/v' curve (or F_M/v curve) is considered to be equal to the total work of fracture needed to split the specimen completely, and is denoted by the term "fracture energy". Dividing this energy by the fracture surface (e.g. in our sample geometry: sample thickness $t \times$ ligament length l) leads to the specific fracture energy, G_F. In addition, the maximum applied horizontal force component, F_{Hmax}, is determined directly from the measured F_M/v curve

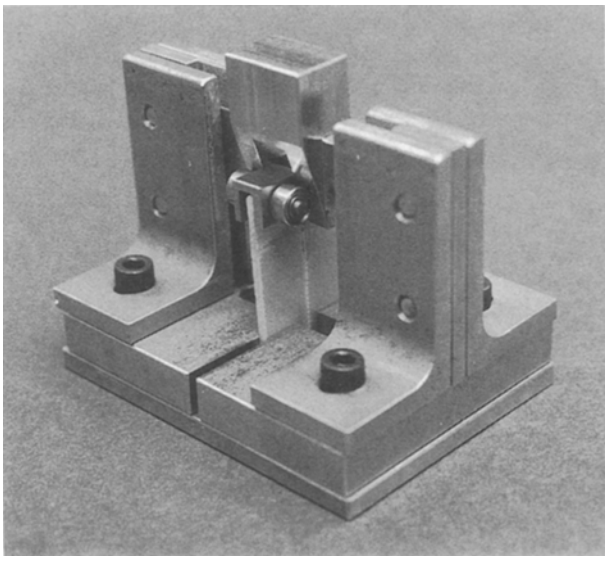

Figure 5 Wedge-splitting device with the specimen in the test position.

using Equation 1. All measurements were done at room temperature and at 77 K.

The load transmission from the wedge on to the specimen was achieved with needle bearings at room temperature and with PTFE (poly-tetrafluorine-ethylene) bearings for testing at 77 K. A "dummy sample" made of steel was used to investigate the influence of friction effects on the measured F_M values for both types of bearings. Compared to the measured F_M values, the friction effects amount to ~2% for the needle bearings and to ~4% for the PTFE bearings and can be neglected.

In addition, acoustic emission (AE) investigations have been made together with the fracture experiments, in order to obtain detailed qualitative information about the fracture process, i.e. the crack initiation point and the AE activity during crack growth. Furthermore, scaling experiments have been made at room temperature to study the influence of the sample

thickness, t, the ligament length, l, and the dimensions, h and w, of the samples on the fracture mechanical quantities. In order to determine average data, four measurements were made on each sample geometry.

4. Results

Typical load–displacement curves (F_M/v) measured on samples with dimensions of $h = 40$ mm, $w = 25$ mm, $t = 2$ mm and a ligament length of $l = 20$ mm, are shown in Fig. 6 for room temperature and 77 K. All test results presented in Table I refer to average values from four measurements, the deviations are always below 5%. The data presented in Table I show an increase of both the maximum horizontal load by a factor of about three (from ~ 500 N at room temperature to ~ 1600 N at 77 K) and the specific fracture energy by about a factor of seven (from ~ 13 N mm^{-1} at room temperature to ~ 95 N mm^{-1} at 77 K).

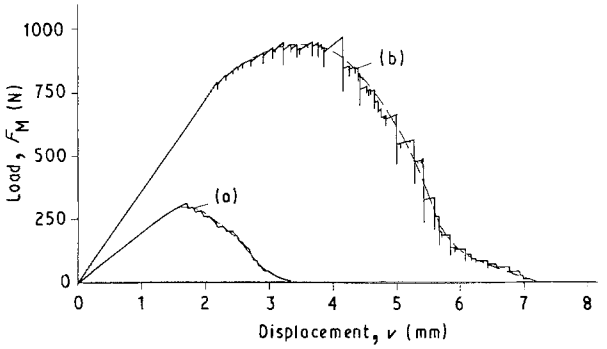

Figure 6 Typical load–displacement curves for samples with a ligament length of 20 mm measured at (a) room temperature and at (b) 77 K.

Fig. 7 shows the results of the AE investigations at room temperature and 77 K recorded during the F_M/v measurements of Fig. 6. The total number of recorded AE events is about the same at both test temperatures, whereas the maximum AE count rates are about three times higher at room temperature.

When testing inhomogeneous materials (e.g. concrete, reinforced plastics), "size effects" are well known and have been investigated in much detail. Earlier investigations [19, 22] on anisotropic fibre-reinforced plastics have shown that specific sample dimensions can, indeed, influence the results on the mechanical quantities. Hence, extensive scaling experiments at room temperature were made in the present study, in order to investigate the influence of all specimen dimensions (Fig. 4a) on the specific fracture energy. Test results pertaining to the influence of the ligament length, l, of the specimen ($h = 50$ mm, $w = 35$ mm) on the specific fracture energy are presented in Fig. 8. With increasing ligament length (from 14 mm to 29 mm) the specific fracture energy increases only slightly ($\sim 5\%$) from ~ 14.5 N mm^{-1} to ~ 15 N mm^{-1}.

TABLE I Test temperatures, average results for the maximum horizontal load, F_H, and the specific fracture energy, G_F, for samples with a ligament length of 20 mm

Temperature (K)	Maximum horizontal load, F_{Hmax} (N)	Specific fracture energy, G_F (N mm^{-1})
293	501	13.3
77	1578	94.6

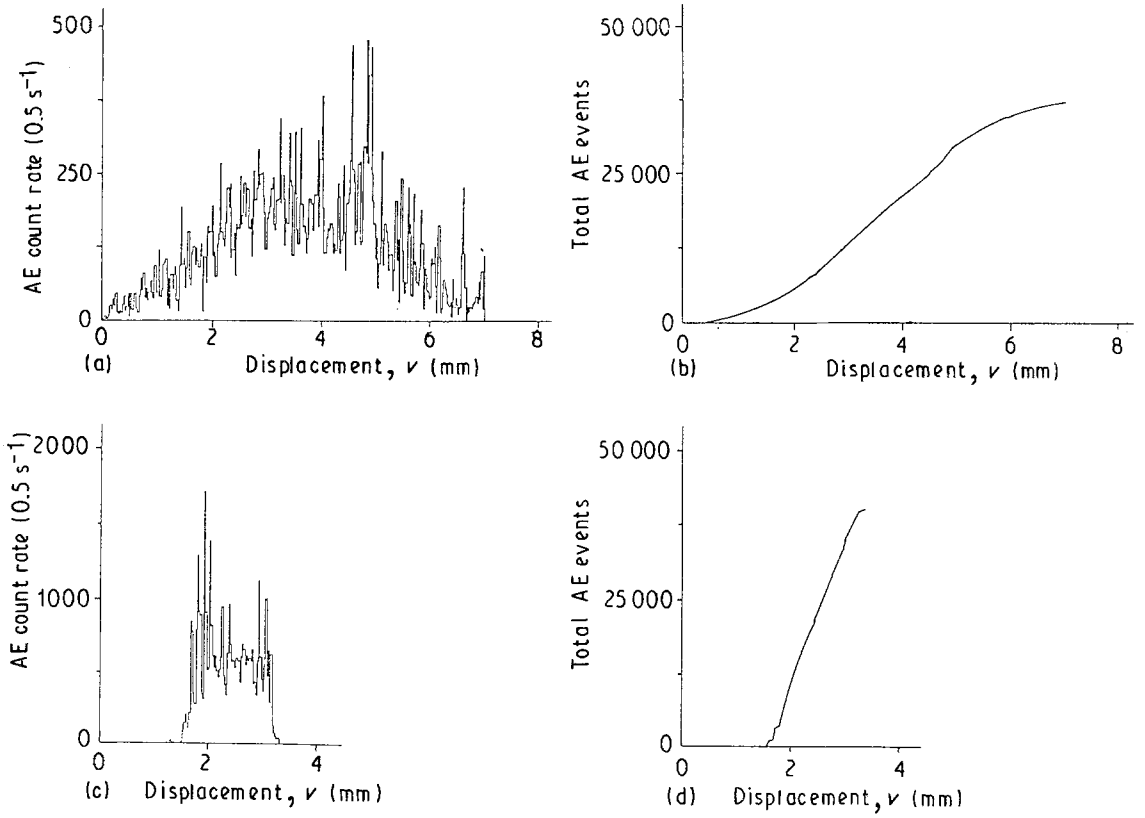

Figure 7 (a, c) AE count rates and (b, d) total number of AE events versus displacement v at (a, b) room temperature and (c, d) 77 K.

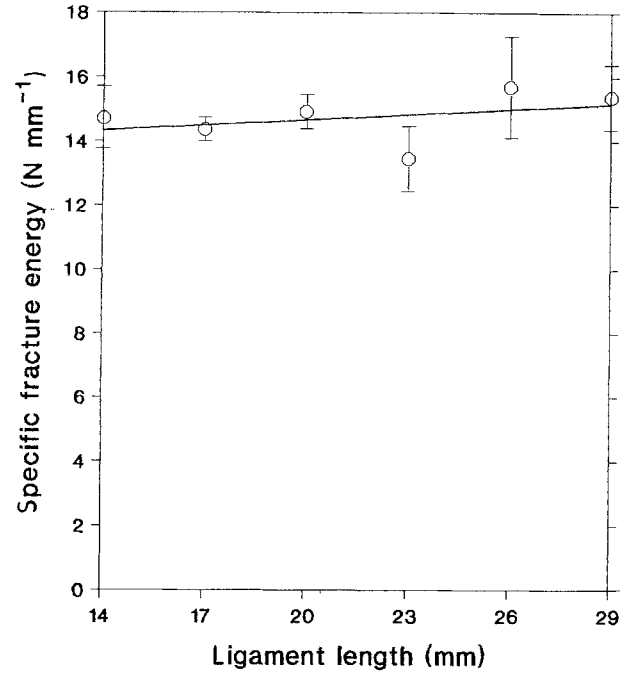

Figure 8 Results for the specific fracture energy versus ligament length at room temperature.

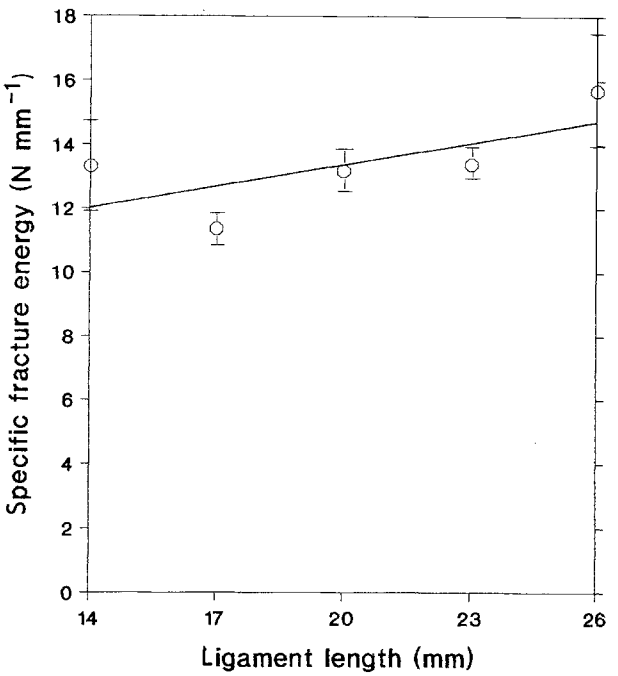

Figure 10 Results for the specific fracture energy versus ligament length for constant notch geometry at room temperature.

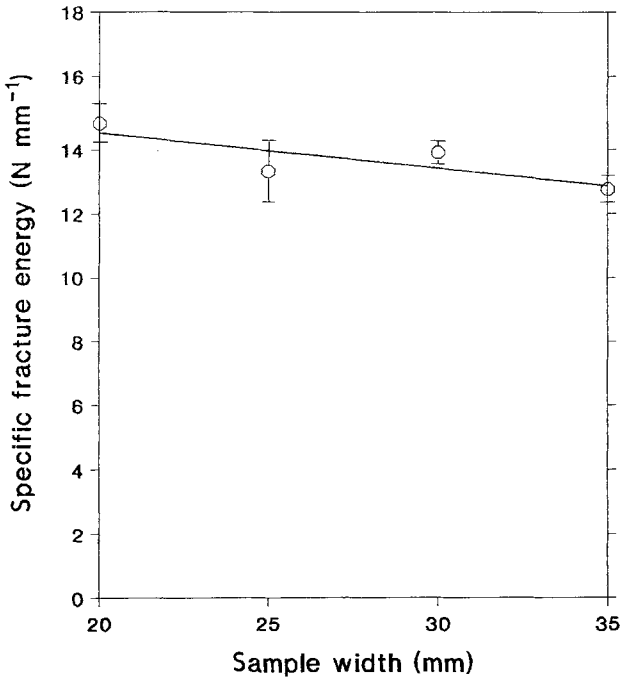

Figure 9 Results for the specific fracture energy versus specimen width at room temperature.

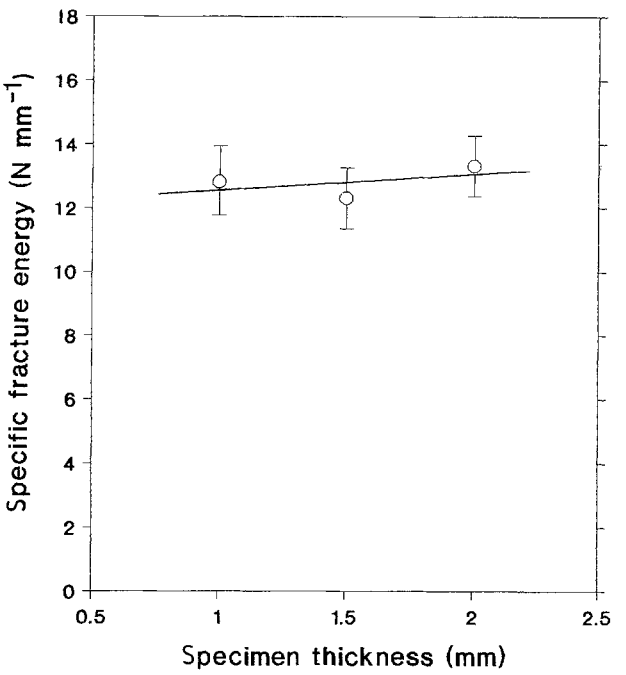

Figure 11 Results for the specific fracture energy versus specimen thickness at room temperature.

The dependence of the specific fracture energy on the sample width, w, of the specimen ($h = 40$ mm, $l = 20$ mm) is plotted in Fig. 9. The specific fracture energy amounts to about 14.5 N mm^{-1} (for samples width $w = 20$ mm) and decreases slightly ($\sim 10\%$) to about 13 N mm^{-1} (for samples width $w = 35$ mm). In another set of experiments, the notch geometry (rectangular groove 6 mm × 9 mm, length of the starter notch 15 mm, Fig. 4a) as well as the sample width, $w = 35$ mm, were kept constant, but the ligament lengths, l, of the specimens were varied. The results are shown in Fig. 10. For specimens with constant notch geometries, the specific fracture energy increases by $\sim 25\%$ from ~ 12 N mm^{-1} (for a ligament length $l = 14$ mm) to ~ 15 N mm^{-1} (for a ligament length $l = 26$ mm). Lastly, the thickness dependence was tested by cutting specimens ($h = 40$ mm, $w = 25$ mm, $l = 20$ mm) from plates with thicknesses of 1, 1.5 and 2 mm. As can be seen in Fig. 11, the specific fracture energy increases only slightly ($\sim 10\%$) from ~ 12.5 N mm^{-1} to ~ 13.5 N mm^{-1} in the thickness range 1–2 mm.

On the basis of the measured load-deformation (F_H/v') curves (F_M/v curves in Fig. 6 and Equations 1 and 2) the strain-softening diagrams of ISOVAL 10 were calculated at room temperature and 77 K using an FEM program given by Roelfstra [15]. The FEM calculation procedure is represented schematically in Fig. 12. At the beginning, the elastic and the "softening" properties of the material are estimated for the uniaxial tensile loading condition and the F_H/v'-curves in Mode I (Fig. 4c) calculated for a sample geometry with $h = 40\,\text{mm}$, $w = 25\,\text{mm}$, $l = 20\,\text{mm}$ and $t = 2\,\text{mm}$ (Fig. 4a). After a comparison of both the calculated and the measured F_H/v' curves, the input parameters are changed and the calculation repeated until good agreement between both the calculated and the measured curves is achieved. The calculated and the experimental F_H/v' curves measured at room temperature are compared in Fig. 13. It will be noted that excellent agreement could be achieved, the deviations being less than 4% (for more details of the FEM program, cf. [15]).

The characteristic material parameters and the bilinear strain-softening behaviour of ISOVAL 10 at room temperature and 77 K are summarized in Table II and Fig. 14, respectively. As can be seen in Fig. 14, the strain-softening behaviour of the material is significantly different at room temperature and at 77 K, respectively.

As an example of our fractographic investigations, a photograph of two test samples (in each case half of the whole sample) following fracture in the crack opening mode (Mode I) at room temperature and 77 K, respectively, is shown in Fig. 15. In the upper part, more "plastic" deformation (larger fracture process zone) can be observed following fracture at 77 K (left side) in comparison to room temperature (right side). As can be seen in the lower part of Fig. 15, only slight delamination occurs at room temperature (right-hand side), whereas delamination becomes

TABLE II Mode I fracture parameters of ISOVAL 10 at room temperature and at 77 K (loading direction 0°/90° with respect to the fibre direction)

		293 K	77 K
G_F	($N\,mm^{-1}$)	14.5	104
σ_0	(MPa)	306	610
s_1	(MPa)	142	268
u_1	(mm)	0.0343	0.126
u_2	(mm)	0.1439	0.492
E	(GPa)	24	36

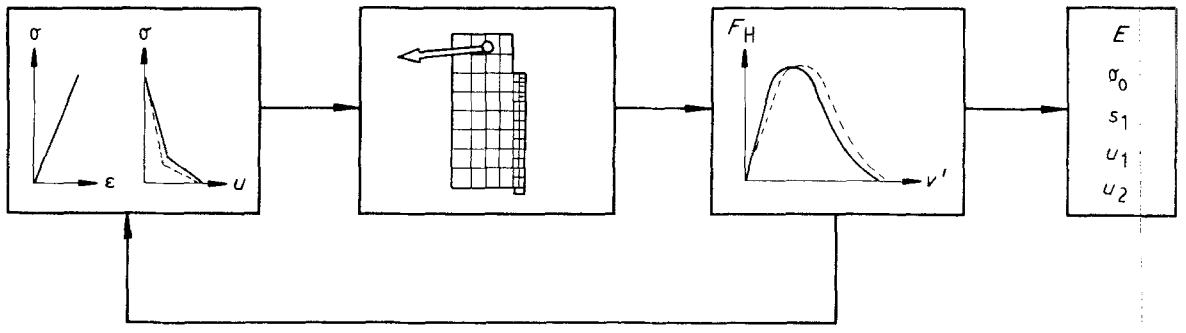

Figure 12 Load-displacement curve and calculated bilinear stress–strain relationship.

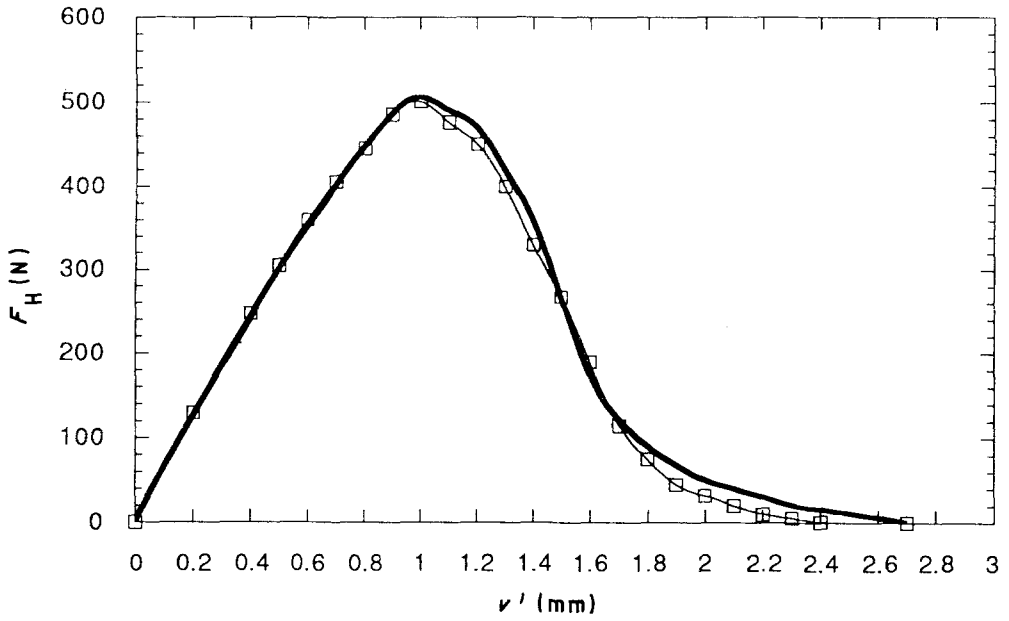

Figure 13 (□) Measured and (——) calculated load-deformation curve at room temperature.

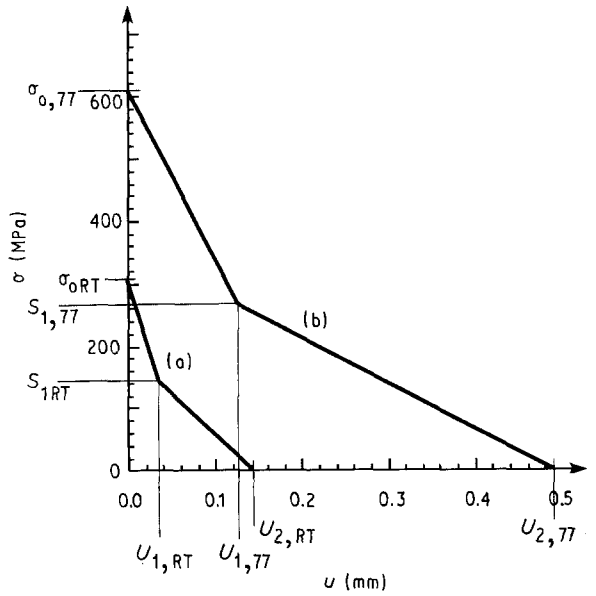

Figure 14 Bilinear strain-softening diagram of ISOVAL 10 at (a) room temperature and (b) 77 K.

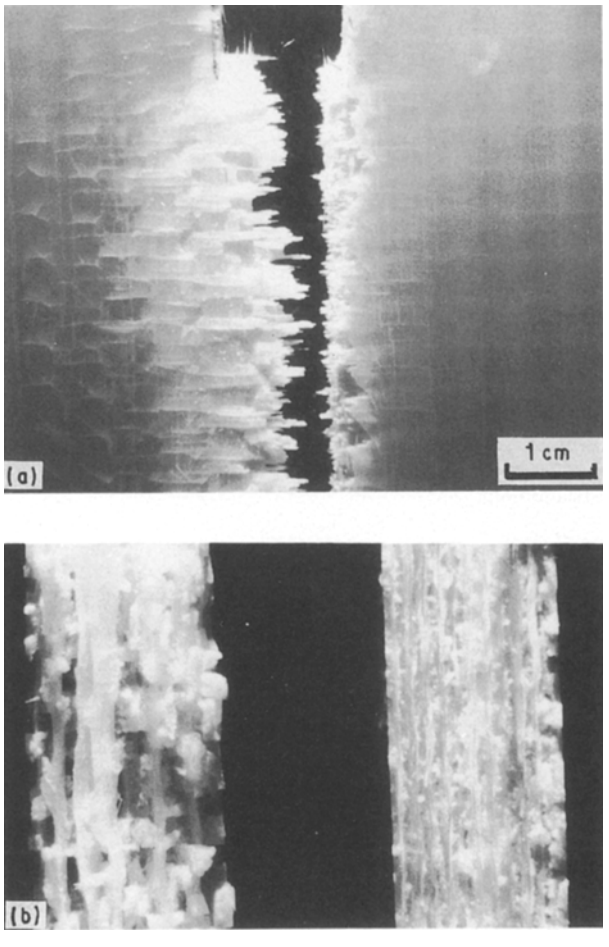

Figure 15 Photographs of (a) the test samples and (b) the fracture surfaces following fracture at room temperature (right-hand side) and at 77 K (left-hand side).

more important at 77 K and the fracture surface shows tufted and brush-like patterns (left-hand side). Additional fractographic examinations with the scanning electron microscope clearly show more fibre/matrix adhesion following fracture at 77 K in comparison to fracture at room temperature (Fig. 16).

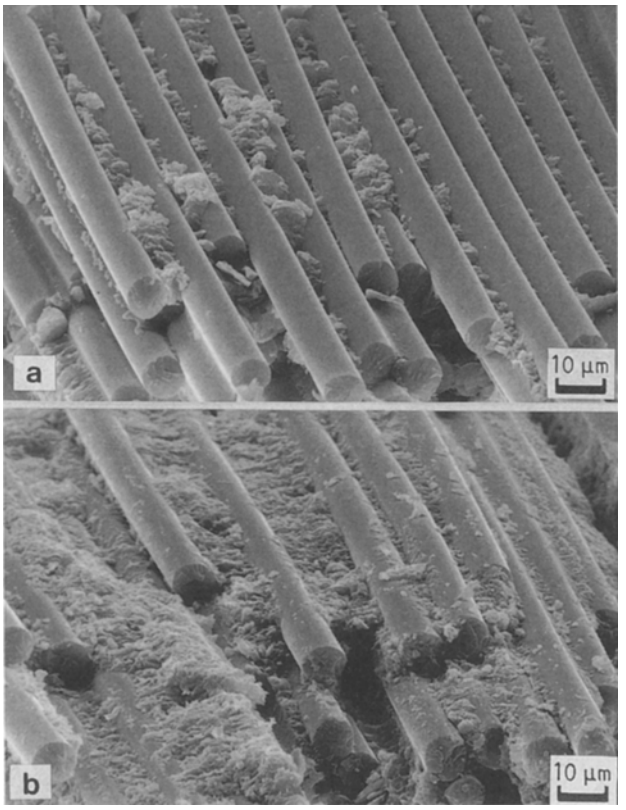

Figure 16 Fibre/matrix interface at the fracture surface following fracture at (a) room temperature and (b) 77 K.

5. Discussion

In the load–displacement curves (F_M/v), two characteristic parts can be distinguished at room temperature and at 77 K, respectively (Fig. 6). Before reaching the maximum load, linear elastic material response prevails at both test temperatures. The F_M/v curve at 77 K shows non-linear material behaviour and a slight "plasticity" shortly before the maximum load is reached. In this part we also find small serrations, which are attributed to the fact, that the matrix becomes more brittle at low temperatures as compared to room temperature, and therefore crazes. At room temperature, the crack initiation takes place when the maximum load is reached. This point of the curve corresponds to the first fibre failure. Then, in the second part of the F_M/v curve, the so-called "softening area", the load drops gradually and the crack propagates under stable crack growth conditions. Because of the broad maximum of the curve (upper part in Fig. 6), the crack initiation and the first fibre failure at 77 K cannot be located exactly. In the second part, the load drops gradually and the crack propagates again under stable crack growth conditions. As compared to room temperature, this "softening area" is more clearly serrated at 77 K. We believe that these serrations reflect the successive pull-out of fibres and fibre fractures during crack propagation.

As pointed out in Section 1, a problem of fracture mechanical tests on fibre-reinforced plastics is the determination of the exact crack length with sufficient

accuracy. In order to avoid this problem, the fracture energy concept [13, 14] was proposed and used in the present study. It does not require the knowledge of the exact crack length for fracture mechanical calculations in contrast to other fracture mechanical concepts (e.g. the *K*-, *G*- or *R*-concept). Starting from the measured F_M/v curves, finite element calculations allow us to determine complete σ/ε curves (Fig. 12), which are needed for a full material characterization and for design purposes. Therefore, the material parameters of ISOVAL 10 given in Table II form an important basis for FEM-calculations of the deformation and fracture behaviour of both unnotched and notched components.

On the other hand, one of the disadvantages of the fracture energy concept lies in the fact that both the specific fracture energy as well as the measured load–displacement curve could depend on the sample geometry, if the sample size is too small. Under these circumstances, the fracture energy could not be called a characteristic material parameter, which must, of course, be independent of sample geometry and size. As a consequence, experiments on the "size effect" have been made at room temperature. The test results show only a slight increase or decrease of the specific fracture energy ($\sim$10%–20%) as a function of ligament length and sample dimensions (Figs 8–10). Furthermore, a "size effect" was observed when increasing the sample thickness from 1 mm to 2 mm. In this case the specific fracture energy increases slightly by about 10% (Fig. 11). This may be explained as follows. A laminate with small thickness consists of only a few layers. The outer layers are less well embedded in the glass-fabric/matrix-compound than the inner layers of the laminate. As a consequence, the outer layers cannot carry the same load as the inner layers. With increasing sample thickness, the percentage of inner layers increases leading to higher values of the specific fracture energy. From a certain sample thickness onwards (number of layers in the laminate), the outer layers can be neglected and the specific fracture energy is nearly constant.

As can be seen in Fig. 15, a larger process zone (more "plastic" deformation) and more delamination occur following fracture at 77 K. As mentioned above, the matrix becomes more brittle at low temperatures, and hence matrix crazes enable the fibres to yield and bend, which results in a larger process zone at 77 K. In addition, the brittleness of the matrix at 77 K leads further to the fact that often the matrix crazes before the fibre/matrix interface fails, and thus, many pieces of the matrix material adhere to the fibre surface (Fig. 16). The so-formed rough fracture surface causes more friction when the broken fibre bundles are pulled out, compared to the smooth fracture surfaces formed at room temperature. Because more energy is needed for pulling out the rough fracture surface as well as for the formation of a larger process zone, the specific fracture energy (being a measure of the resistance against crack propagation) is higher at 77 K (i.e. by about a factor of seven, Table I).

The results of the AE investigations (Fig. 7) are different at both test temperatures. At room temperature, no AE events occur before crack initiation takes place. Beginning from this moment, peaks in the AE count rates are recorded, which correspond accurately to the serrations of the load–displacement curve (Fig. 6). At 77 K (Fig. 7), the AE count rates increase remarkably, when the load–displacement curves become non-linear. The brittleness of the matrix leads to matrix crazing, which results in these AE signals. After the crack initiation point, all further peaks in the AE count rates are again related to the serrations in the load–displacement curve. Hence, a more continuous distribution of the AE activity can be observed at 77 K than at room temperature.

Finally, advantages and disadvantages of the new test method should be discussed. The test method and the device are experimentally simple and the test can be done in all top-loading cryostats suitable for tensile test machines with a force-reversal arrangement. Furthermore it should be pointed out that the sample mounting is simple (especially important for irradiated samples!) and the sample preparation quick and cheap. On the other hand, the fact that a minimum sample size is necessary to avoid buckling, and secondly, that the evaluation requires finite element calculations for the determination of real material parameters (stress–strain curve) from the load–displacement curve (Fig. 12) can be considered as certain disadvantages of the method.

6. Conclusions

As pointed out in Section 1, the assessment of fracture mechanical properties of fibre-reinforced plastics in the crack-opening-mode (Mode I) is of considerable interest for many applications. Several different sample geometries have been proposed for Mode I tests on fibre-reinforced plastics in the past, but no test method has received general acceptance or is suitable for all measurements, especially at cryogenic temperatures and on irradiated samples. In this paper a new splitting test technique has been proposed for the characterization of fracture mechanical material properties in the crack opening mode (Mode I), which is based on the fracture-energy concept. This allows us to determine complete σ/ε curves by means of finite element calculations.

The main results obtained on a fibre-reinforced plastic (ISOVAL 10) may be summarized as follows.

1. The test method and the device are experimentally simple and the test can be done in a wide range of temperatures including cryogenic temperatures on irradiated and unirradiated samples.

2. The fracture-energy concept does not require the knowledge of the exact crack length. The recorded load–displacement curves contain all the information needed for a full material characterization.

3. With decreasing test temperature from room temperature down to 77 K, both the specific fracture energy and the maximum load increase (by factors of seven and four, respectively) for the material investigated in the present study.

4. The load–displacement curves show linear elastic material behaviour at the beginning and serrations

(more clearly at 77 K) in the second part of the curves (softening area).

5. The peaks in the acoustic-emission count rates are accurately correlated with the serrations of the load–displacement curve. More uniform acoustic-emission activity is observed at 77 K.

6. Scaling investigations have shown only a slight dependence of the specific fracture energy ($\sim 10\%$) on the ligament length as well as on the sample and notch dimensions.

7. Fractographic examinations have shown more "plastic" deformation (larger fracture process zone) and fibre/matrix adhesion following fracture at 77 K in comparison to fracture at room temperature.

8. On the basis of the measured load–deformation curves, the strain-softening behaviour of the material can be determined with FEM. All material parameters necessary for numerical calculations of the fracture behaviour in Mode I can be taken directly from the strain-softening diagram. Therefore, they represent intrinsic material parameters.

Acknowledgements

The authors thank ISOVOLTA AG, Wiener Neudorf, Austria, for providing us with the test samples of ISOVAL 10. Finite element calculations by Mr M. Zelezny and technical support by Mr H. Niedermaier and Mr E. Tischler are acknowledged. This work was supported in part by Bundesministerium für Wissenschaft und Forschung, Vienna, under contract 77.780/2-25/91.

References

1. H. LAU, H. H. ABDELMOHSEN and M. K. ABDELSALAM, *Adv. Cryog. Engng* **34** (1988) 83.
2. S. M. LEE, *J. Compos. Mater.* **20** (1986) 185.
3. S. HASHEMI, A. J. KINLOCH and J. G. WILLIAMS, *Compos. Sci. Tech.* **37** (1990) 429.
4. *Idem, Proc. R. Soc. Lond. A* **427** (1990) 173.
5. A. C. GARG, *Engng Fract. Mech.* **23** (1986) 719.
6. A. C. GARG and O. ISHAI, *ibid.* **22** (1985) 413.
7. *Idem, ibid.* **22** (1985) 595.
8. Y. KAGAWA, E. NAKATA and S. YOSHIDA, ASTM STP 864 (American Society for Testing and Materials, Philadelphia, PA, 1985) p. 27.
9. A. DAIMARU, T. HATA and M. TAYA, *ibid.* p. 505.
10. S. M. JENG, J. M. YANG and C. J. YANG, *Mater. Sci. Engng A* **138** (1991) 181.
11. C. G. ARONSSON and J. BÄCKLUND, *J. Compos. Mater.* **20** (1986) 287.
12. *Idem*, ASTM STP 907 (American Society for Testing and Materials, Philadelphia, PA, 1986) p. 134.
13. A. HILLERBORG, in Proceedings of "Fracture Mechanics of Concrete, Developments in Civil Engineering", Vol. 7 edited by F. Wittmann (Elsevier, Amsterdam, 1983) p. 223.
14. *Idem, Mater. Construct.* **18** (1985) 25.
15. P. E. ROELFSTRA, Thesis, Ecole Polytechnique Federale de Lausanne (1989).
16. B. HILLEMEIER, Thesis, University of Karlsruhe (1976).
17. E. K. TSCHEGG, Aust. Pat. 233/86, 390 328 (1986).
18. *Idem, Mater. Test.* **33** (1991) 338.
19. E. K. TSCHEGG, K. HUMER and H. W. WEBER, *Adv. Cryog. Engng* **38A** (1992) 355.
20. H. N. LINSBAUER and E. K. TSCHEGG: Final report A1, COST 502, No. HNL-01-89 (1989).
21. E. K. TSCHEGG, *ASTM J. Test. Eval.* (1991) submitted.
22. E. K. TSCHEGG, K. HUMER and H. W. WEBER, *Cryogenics* **31** (1991) 312.

Received 12 May
and accepted 12 October 1992